

Prediction of huge magnetic anisotropies of transition-metal dimer–benzene complexes

Ruijuan Xiao, Daniel Fritsch,* Michael D. Kuz'min, Klaus Koepernik, and Manuel Richter

IFW Dresden e.V., PO Box 270116, D-01171 Dresden, Germany

Knut Vietze and Gotthard Seifert

Physikalische Chemie, Technische Universität Dresden, D-01062 Dresden, Germany

(Dated: September 3, 2010)

Abstract

Based on numerically accurate density functional theory (DFT) calculations, we systematically investigate the ground-state structure and the spin and orbital magnetism including the magnetic anisotropy energy (MAE) of 3d- and 4d-transition-metal dimer benzene complexes (TM_2Bz , $\text{TM} = \text{Fe}, \text{Co}, \text{Ni}, \text{Ru}, \text{Rh}, \text{Pd}$; $\text{Bz} = \text{C}_6\text{H}_6$). These systems are chosen to model TM-dimer adsorption on graphene or on graphite. We find that Fe_2 , Co_2 , Ni_2 , and Ru_2 prefer the upright adsorption mode above the center of the benzene molecule, while Rh_2 and Pd_2 are adsorbed parallel to the benzene plane. The ground state of Co_2Bz (with a dimer adsorption energy of about 1 eV) is well separated from other possible structures and spin states. In conjunction with similar results obtained by *ab initio* quantum chemical calculations, this implies that a stable Co_2Bz complex with C_{6v} symmetry is likely to exist. Chemical bonding to the carbon ring does not destroy the magnetic state and the characteristic level scheme of the cobalt dimer. Calculations including spin-orbit coupling show that the huge MAE of the free Co dimer is preserved in the Co_2Bz structure. The MAE predicted for this structure is much larger than the MAE of other magnetic molecules known hitherto, making it an interesting candidate for high-density magnetic recording. Among all the other investigated complexes, only Ru_2Bz shows a potential for strong-MAE applications, but it is not as stable as Co_2Bz . The electronic structure of the complexes is analyzed and the magnitude of their MAE is explained by perturbation theory.

PACS numbers: 31.15.es, 75.30.Gw, 75.75.-c

* present address: School of Physics, Trinity College Dublin, Dublin 2, Ireland.

I. INTRODUCTION

Motivated by the ongoing quest for yet higher-density magnetic data storage in the context of the rapid advance of information technology, there is a continued search for nanoscopic magnetic structures with a large magnetic anisotropy energy (MAE) density by different experimental^{1–6} and theoretical^{7–15} methods. The MAE is the energy needed to turn the saturated magnetization of a system from one direction, usually the ground-state orientation, to another high-symmetry direction. Talking for simplicity about a nanoscopic system, we mean a canonical statistical ensemble of such systems, i.e. a macroscopically large number of identical non-interacting systems at equilibrium with a thermal bath.

Thus, the MAE describes the stability of the magnetization direction against differently oriented external magnetic fields. In the simplest case of uniaxial anisotropy with an easy axis, the MAE is the energy barrier between two opposite equivalent directions of magnetization with the lowest energy. A well-known example for this situation is bulk *hcp* Co. Using the bi-stability of magnetic structures, a bit of information can be stored: for example, one stable direction of magnetization on a hard disc area may encode “0”, the other stable direction “1”. It is generally accepted that long-term data storage requires that the total MAE of each magnetic particle should exceed $40\ kT$,¹⁶ where k is the Boltzmann constant and T is the temperature.

Spin-orbit interaction in a magnetic state is the primary source of MAE.¹⁷ The size of the spin-orbit coupling parameter of a given shell is a merely atomic property that depends on the atomic number. Hence, the spin-orbit splitting of atomic, molecular, or band states is fully determined by the character of these states in terms of atomic orbitals. On the other hand, the MAE as an energy difference depends sensitively on the particular electronic structure and, thus, on the geometry of the system. For instance, bulk *hcp* Co shows a moderate MAE of 0.06 meV per atom. Larger MAE can be obtained in surface-supported structures. It can be considerably influenced by tuning the coordination and the hybridization through the choice of substrate and size of the deposited clusters. For instance, the deposition of single Co atoms on a Pt(111) surface yields a record MAE of 9 meV per Co atom.¹

Further reduction of the dimensions leads into the realm of nano-particles and magnetic molecules. To give an example, Fe₄ organometallic clusters with a propeller-like structure exhibit magnetic anisotropy barriers which can be tuned by altering the ligands and reach

up to 1.5 meV per cluster.² A large anisotropy barrier of 7 meV per cluster, generated by a deliberate structural distortion of the magnetic core with the help of bulky organic ligands, was recently reported for a complex within the Mn_6 family of single-molecule magnets.³

Isolated magnetic dimers are the smallest chemical objects that possess a magnetic anisotropy as their energy depends on the relative orientation between dimer axis and magnetic moment. Huge MAE values of up to 100 meV per atom were predicted for several transition-metal dimers (Ti_2 , Fe_2 , Co_2 , Ni_2 , Zr_2 , Tc_2 , Rh_2 , Ir_2 , and Pt_2).^{8,11,18,19} However, it is impossible to utilize the huge MAE of dimers technologically unless they are bound to some medium. Our recent studies demonstrate that carbon-based substrates are suitable for this purpose.¹⁴ Both benzene (Bz) and graphene are ideal support materials that do not spoil magnetism and the huge MAE of the Co dimer. The Co_2Bz complex has a ground-state structure with C_{6v} symmetry, in which the dimer is bound perpendicularly to the carbon plane. This hexagonal environment preserves the two-fold degenerate singly occupied highest molecular orbital (HOMO) of the free Co dimer, which is responsible for the large dimer MAE.⁸ As a result, Co_2Bz was predicted to show a magnetic anisotropy of the order of 100 meV per molecule.¹⁴ This finding may open a way to enhance the presently available area density of magnetic recording by 3 orders of magnitude.

The present work has two aims. First, additional detailed results on Co_2Bz will be presented that support the conclusions drawn in Ref. 14. Second, related results for a whole series of dimer-benzene complexes including the 3d and 4d dimers Fe_2 , (Co_2), Ni_2 , Ru_2 , Rh_2 , and Pd_2 will be shown. Among these, only Co_2Bz and Ru_2Bz turn out to be interesting candidates for a potential strong-MAE application.

Benzene-reacted metal dimers have been explored since the 1980s. Trevor *et al.*²⁰ studied the reaction products of benzene with gas-phase platinum clusters of different size. The existence of Fe_2Bz was verified with infrared spectroscopy by Ball *et al.*²¹ after the reaction of iron atoms with cyclic hydrocarbons in an argon matrix. More recently, Bowen's group performed a series of mass spectrometry and photoelectron spectroscopic studies on iron-benzene,²² iron-coronene,²³ cobalt-benzene,²⁴ cobalt-pyrene,²⁵ cobalt-coronene,²⁶ and nickel-benzene²⁷ cluster anions. The electron affinities and the vertical electron detachment energies were extracted from experimental spectra for the above complexes. By comparing measured spectra with results of density functional theory (DFT) calculations,^{23,26} they proposed structure models for a part of these clusters. For example, a half-sandwich ground-

state structure (C_{6v} symmetry) was postulated for Fe_2Bz^- .²² Their investigations suggest that carbon rings could be a suitable template to deposit small transition-metal clusters. The reaction of Rh_n^+ cations with benzene was studied by Berg *et al.*²⁸ These authors found that for $n = 2$ small amounts of Rh_2Bz^+ were formed, while the main products were $\text{RhBz}^+ + \text{Rh}$ and $\text{Rh}_2\text{C}_6\text{H}_4 + \text{H}_2$. Lüttgens *et al.*²⁹ measured the photoelectron detachment spectra of M_2Bz^- ($\text{M} = \text{Pt}, \text{Pd}, \text{Pb}$) and resolved the electron affinities and ground-state vibration energies of these complexes. By analyzing the vibration frequencies, they postulated a perpendicular arrangement of Pd and Pt dimers on Bz (C_{6v} symmetry) and a parallel coordination between Pb_2 and Bz (C_{2v} symmetry).

On the theoretical side, DFT calculations were performed on several transition-metal benzene systems. Considering reaction products of iron atoms and benzene in low-temperature matrices, Parker recently calculated the energy of a number of isomers and simulated the related infrared spectra.³⁰ By comparison of calculated and measured spectra he concluded that Fe_2Bz is formed at high iron concentrations. If the Fe dimer is assumed perpendicular to the benzene plane above the center of the carbon ring, the calculated infrared spectrum shows an excellent agreement with the experimental data, though the calculation finds a different ground-state isomer.

The ground-state structures of Fe_2 -coronene,²³ Co_2 -pyrene,²⁵ and Co_2 -coronene²⁶ were also studied. For Fe_2 -coronene, a ground state with a total spin $S = 3$ was found with three quasi-degenerate isomers, where the Fe dimer is oriented either parallel or perpendicular to the coronene plane.²³ For both Co_2 -pyrene and Co_2 -coronene, the ground state was found to be $S = 2$ with perpendicular orientation of the Co dimer at a position above a peripheral C-C bridge.^{25,26} Earlier work in this field is due to Senapati *et al.*³¹ who studied neutral and cationic Fe_2 -coronene complexes but discussed only parallel adsorption modes. Also, Rao and Jena studied the geometries and magnetic moments of neutral and ionic Ni_nBz_m complexes.^{32,33} They predicted a parallel adsorption mode between the Ni dimer and benzene, but it is unclear whether a perpendicular geometry was considered or not. The interaction of benzene with Rh^+ and with Rh_2^+ was investigated by Majumdar *et al.*³⁴ For the physisorbed dimer cation, Rh_2Bz^+ , the minimum energy geometry has C_{2v} symmetry with the two rhodium atoms lying horizontally above the benzene at the C-C bridge sites.

Further research activities were devoted to transition-metal dimers interacting with

graphene or with fullerenes. Interaction of silver and gold adatoms and dimers with graphite or graphene was studied,^{35,36} and a perpendicular orientation of gold dimers on graphene was predicted.³⁶ Also, both structure and spin magnetic properties of 3d transition-metal adatoms and dimers on graphite were investigated by Duffy *et al.*,³⁷ but a possible perpendicular arrangement of the dimers was not considered. DFT calculations for palladium clusters supported on graphene³⁸ and on C₆₀³⁹ find that the two atoms of an adsorbed Pd dimer are located on bridge sites, i.e., on top of C-C bonds. Recently, two detailed theoretical studies of Fe, Co, and Ni adatoms and dimers adsorbed on graphene were published: Johll *et al.*⁴⁰ found that the most stable structure for all considered dimers, Fe₂, Co₂, and Ni₂, has a dimer axis oriented perpendicularly to the graphene plane and placed at the hole site. An enhancement of the magnetic moment for the atom farther from the graphene was predicted,⁴⁰ compared with the free dimer. Cao *et al.*⁴¹ found the same ground-state geometry, if the density-gradient corrected functional according to Perdew, Burke, and Ernzerhof⁴² was used, but they note that partly different results were obtained by using the local spin-density approximation (LSDA).

DFT calculations do not only allow to predict the ground-state geometry and spin of a magnetic complex, but may also provide a basic understanding of the electronic structure and of the orbital magnetic properties like orbital magnetic moment and MAE. We are however not aware of any published calculations of the magnetic anisotropy of transition-metal dimers on carbon-based systems except our recent letter, Ref. 14. In the following, we will demonstrate by DFT calculations that carbon hexagons are suitable hosts, where adsorbed transition-metal dimers may preserve their exceptional magnetic anisotropy.

The investigated TM₂Bz complexes are meant to serve as model structures for the adsorption of transition-metal dimers on the surface of graphite, on graphene, or on other carbon structures including molecular systems. For this reason, we only consider so-called physisorption (adsorption without expelling other atoms, e.g., hydrogen) as opposed to chemisorption that includes the possibility of de-hydrogenation.³⁴ Most probably, the presented predictions can only be verified under ultra-high vacuum conditions. Any interaction of the transition-metal atoms with, e.g., oxygen may deteriorate the specific structure and the related magnetic state we are focusing on.

The paper is organized as follows. In Sec. II, the calculation method and computational details are explained. Sec. III compiles all results and related discussion: structure opti-

mization and stability of the ground states, analysis in terms of the bonding mechanism, the spin and orbital moments, and the strength of the MAE. The origin of the huge MAE in some of these molecules is also explained. Finally, the paper is summarized in Sec. IV. The appendix contains a description of auxiliary calculations.

II. METHOD AND COMPUTATIONAL DETAILS

The DFT calculations were performed with an highly accurate all-electron full-potential local-orbital scheme (FPLO),⁴³ release 8.00-31.⁴⁴ The code is based on a linear combination of overlapping nonorthogonal orbitals with a compact support. The molecular mode of FPLO with free boundary conditions was used. The presented data were obtained using the generalized gradient approximation (GGA) with a parameterized exchange-correlation functional according to Perdew, Burke, and Ernzerhof.⁴² All results were checked against additional calculations using the LSDA in the parameterization by Perdew and Wang.⁴⁵ The dimer adsorption energy calculated by GGA is in all cases about 1 eV smaller than the related LSDA energy, but both approaches find the same ground-state structure type. Also, the ground-state spin obtained with GGA or LSDA is the same for all systems except Rh₂Bz, where LSDA yields a non-magnetic ground state and GGA yields an $S = 1$ ground state. In both cases, however, the energies of the $S = 0$ and $S = 1$ states are very close.

The molecular levels were occupied according to a Fermi-Dirac distribution in order to ensure the convergence of the Kohn-Sham equations. The presented results were obtained with a broadening temperature of $T = 100$ K. The basis set comprised 3d-transition-metal (3s, 3p, 3d, 4s, 4p, 4d, 5s), 4d-transition-metal (4s, 4p, 4d, 5s, 5p, 5d, 6s), carbon (1s, 2s, 2p, 3s, 3p, 3d), and hydrogen (1s, 2s, 2p) states. Lower-lying states of the transition-metal atoms were treated as core states.

Geometry optimization was carried out with a scalar relativistic scheme. To find out the lowest-energy geometry and spin magnetic state of each TM₂Bz complex, three possible high-symmetry structures (Fig. 1) were optimized for $S = 0, 1, 2$, and 3 (total spin moment, $\mu_S = 0, 2, 4$, and $6\mu_B$), and for different initial spin arrangements (ferro- and ferrimagnetic). The point group symmetry C_{6v} was applied for the configuration shown in Fig. 1(a), while for the structures depicted in Figs. 1(b) and 1(c), C_{2v} was used for the structure optimization.

Previous theoretical investigations of metal-benzene systems have shown that the struc-

tural changes of the benzene plane due to the metal-benzene interaction are negligible.^{9,46–48} Thus, in nearly all our calculations the positions of the C and H atoms were fixed with C-C bond length 1.40 Å and C-H bond length 1.09 Å. Exceptions from this strategy are reported below.

The Co₂Bz complex is of particular interest.¹⁴ To make sure that the correct ground state was found for this system, we utilized the pseudopotential code ESPRESSO-4.0.1⁴⁹ and cross-checked the above calculations by full optimization of all the atomic positions starting from 14 kinds of initial structures. The computational details and a brief description of the results are given in the appendix.

A quantity used to judge the stability of the considered structures is the adsorption energy (E_{ad}) for a dimer entity attached to a benzene molecule, which is defined as

$$E_{ad} = E_{tot}(\text{Bz}) + E_{tot}(\text{TM}_2) - E_{tot}(\text{TM}_2\text{Bz}) . \quad (1)$$

Here E_{tot} refers to the respective total energy of the species indicated in the parentheses. Negative values of E_{ad} mean that the TM₂Bz complex is unstable.

To evaluate the orbital magnetic moment and the MAE, spin-orbit coupling has to be included in the calculation. However, standard (quasi-)local DFT approximations like LSDA or GGA do not include orbital-dependent exchange effects.⁵⁰ Thus, the orbital moments and the MAE are usually underestimated by these approaches. The orbital polarization (OP) correction⁵¹ is a frequently applied method to cure this problem. As a matter of experience, the MAE evaluated with standard LSDA or GGA approximation gives a lower estimate to the expected MAE, while the value obtained by including the OP correction provides an upper estimate. Experimental values of the MAE are most probably located between these lower and upper estimates. This has been demonstrated, e.g., in Refs. 52 and 7 and also for the special case of Co atoms in different chemical and structural surroundings in Ref. 14, Fig. 3.

The MAE and the orbital magnetic moment were calculated by means of self-consistent fully relativistic calculations using the bond lengths obtained in the scalar relativistic calculations. The MAE was defined as

$$\text{MAE} = E_{tot}[\parallel] - E_{tot}[\perp] , \quad (2)$$

where $E_{tot}[\parallel]$ and $E_{tot}[\perp]$ denote total energies of states with magnetization direction parallel and perpendicular to the Bz plane, respectively. The choice of the direction parallel to the

plane is arbitrary, since the in-plane anisotropy is negligible on the scale of the considered energies. Results obtained with and without OP corrections are reported. In the former case, the spin-dependent OP correction⁵³ was applied to the $3d$ -orbitals of Fe, Co, Ni and to the $4d$ -orbitals of Ru, respectively.

In order to cross-check one of the most important details of the GGA calculations, the bonding behavior of the Co dimer with Bz, we also performed *ab initio* quantum chemical calculations at the level of second order Møller-Plesset perturbation theory (MP2). The MP2 results were obtained from the MP2 implementation of Gaussian03.⁵⁴ For Co₂Bz, the Co atoms were described with a scalar-relativistic effective core potential (ECP) replacing 10 core electrons (MDF10),⁵⁵ with the corresponding $(8s7p6d\ 1f)/[6s5p3d\ 1f]$ GTO basis set of triple-zeta quality. Accordingly, for benzene the Dunning correlation-consistent basis sets of double- and triple-zeta quality (cc-pVDZ and cc-pVTZ, respectively)⁵⁶ were used. Since all of these basis sets are rather large, all energies have been corrected for the basis set superposition error (BSSE) with respect to the dissociation of the Co dimer from the benzene ring, employing the counterpoise scheme proposed by Boys and Bernardi^{57,58} as implemented in Gaussian03.

III. RESULTS AND DISCUSSION

A. Structure and spin state

Dimer adsorption energies for each considered total spin and symmetry are shown in Fig. 2. The optimized structure parameters, dimer adsorption energies, and related spin magnetic moments for the six ground-state structures are listed and compared with literature data in Table I.

1. $3d$ transition-metal complexes

We find that the adsorption mode with the dimer axis perpendicular to the benzene plane results in the most stable structure for all investigated $3d$ systems, Fe₂Bz, Co₂Bz, and Ni₂Bz. This ground-state geometry is consistent with other GGA results obtained for dimers on graphene.^{40,41} The only discrepancy occurs for the ground-state spin magnetic moment of Fe₂Bz. Here, we found a reduction of the free dimer spin ($S = 3$) to $S = 2$,

whereas Johll *et al.* and Cao *et al.* had reported $S = 3$ for the marginally different situation of Fe₂ on graphene.^{40,41} As the related energy difference in our calculation was very small (9 meV), we repeated the calculations with full optimization of the C-C and C-H distances (C_{6v} symmetry). The full optimization inverted the order of the two considered states, the state with $S = 3$ now being 16 meV lower than the competing state with $S = 2$. Moreover, a ferrimagnetic state with $S = 1$ is found only about 40 meV higher in energy, Fig. 2. Such small energy differences cannot guarantee the stability of the Fe₂Bz magnetic ground state and should give rise to strong spin fluctuations.

Turning our attention to the ground-state geometry of Fe₂Bz, we note that Parker³⁰ provided evidence of the same proposed geometry by obtaining an excellent agreement between calculated and experimental infrared spectra. Note, that in this geometry Fe₂Bz complexes with $S = 1, 2$, and 3 give almost identical simulated spectra.³⁰ Thus, the comparison cannot be used to distinguish the magnetic state. Our results add additional weight to Parker's arguments, who proposed a C_{6v} geometry for Fe₂Bz. One should note, however, that other structure types compete with the C_{6v} geometry, see Fig. 2. Indeed, if the C and H coordinates are optimized as well, the ground state turns to \parallel_b , $S = 3$, almost degenerate with the states \perp_c , $S = 2$ and $S = 3$. In line with this finding, Cao *et al.* reported a ground state with the Fe dimer above a graphene hollow site, but not perpendicular to the plane.⁴¹ In the following discussion, we will disregard Fe₂Bz structures different from C_{6v} due to the mentioned experimental evidence of this structure type.

For Co₂Bz and Ni₂Bz, we obtained both the magnetic moment and the ground-state structure in agreement with the results by Johll *et al.*⁴⁰ and by Cao *et al.*⁴¹ The GGA dimer adsorption energy, $E_{ad} = 1.39$ eV for Co₂ on Bz from our calculation, and the related energies 0.92 eV from Johll *et al.* and 1.13 eV from Cao *et al.* for Co₂ on graphene indicate a reasonable stability of this structure. Noteworthy, any other spin state considered in our calculations, including a ferrimagnetic solution with a total spin $S = 1$, has a much higher energy, at least 0.80 eV above the ground state. The ground state of Ni₂Bz is also sufficiently separated from other states with a different spin and/or geometry, see Fig. 2. We also checked a further geometry with Ni atoms close to next nearest C-bridges (see Fig. A1 (iv)). Such a geometry was found by Rao and Jena³³ to be lowest in energy. We could not confirm this finding and obtained, even with full relaxation, a 0.45 eV higher energy for this geometry ($S = 1$) than for the \perp_c geometry with $S = 1$.

To investigate the stability of the proposed perpendicular adsorption mode for the Co system in more detail, three further structures were considered, including two dissociated cases: (i) attachment of one Co atom on each side of the carbon ring, (ii) dissociation of one of the Co atoms resulting in one free Co atom and CoBz, and (iii) dissociation of both Co atoms resulting in two free Co atoms and one free benzene molecule. In the related scalar relativistic atom calculations, non-integer occupation of the open shells was admitted. All the three structures have higher energies, by 2.47 eV, 3.49 eV, and 5.05 eV, respectively, than the perpendicular arrangement. From the energy difference between state (ii) and state (iii), a value of 1.56 eV is found for the adsorption energy of a single Co adatom on benzene. We also can find a binding energy of 3.66 eV for the Co dimer from the third dissociated state. In comparison with the DFT data, the experimental binding or adsorption energies are considerably smaller: 0.34 eV⁵⁹ (adsorption energy of a Co adatom to benzene) and 1.72 eV⁶⁰ (binding energy of a Co dimer). This is in line with the known tendency of DFT calculations to overestimate the binding energies in many cases.

Thus, to confirm the qualitative validity of the energies and structure sequence, we performed quantum chemical (MP2) calculations. In comparison with our previously published results,¹⁴ the MP2 calculations were improved by taking into account BSSE corrections and by extending the benzene basis. Fig. 3 compares the energy sequences of three possible high-symmetry structures and one dissociated configuration obtained by GGA with related MP2 results. All MP2 energies were evaluated by single point calculations using the GGA-derived geometries, except for the Co dimer. For the latter the interatomic distance was optimized at the MP2 level. It turned out slightly shorter (0.1909 nm) than the GGA result (0.1997 nm). For all structures, MP2 calculations were carried out for $S = 0, 1, 2$ and 3. In all cases a total spin of 2 was found to be most favorable. Importantly, the adsorption energy of the Co dimer to benzene was found to be yet higher than in the GGA calculation. It is obvious from Fig. 3 that the quantum chemical calculations confirm the main GGA result, that bonding of a Co dimer with a single molecule of benzene results in the structure depicted at the bottom of Fig. 3 with a total spin $S = 2$. Also, the sequence of the higher-energy structures is the same in GGA and in MP2, and the same spin magnetic moments are found with the exception of the dissociated state, where MP2 predicts $S = 3$ and GGA yields $S = 2$. When improving the benzene basis from a double- to a triple-zeta level, the BSSE-corrected adsorption energies rise consistently by about half an eV, reaching 2.36 eV

for the most stable structure. This result should serve as a valid proof that the Co dimer can be bound to the benzene ring.

As a final check that the calculations described above provided the correct ground-state geometry, we performed a cross-check for Co_2Bz with the pseudopotential code ESPRESSO-4.01.⁴⁹ We carried out a full optimization of all atomic positions starting from 14 kinds of initial structures. As before, GGA and a scalar relativistic mode were used. Other technical details are described in the appendix. The results confirm that the bonding of Co_2 with a single molecule of benzene very likely results in the perpendicular configuration, which is separated from other possible arrangements by at least several hundred meV. Only a tiny distortion of the benzene plane is found in the full optimization results. This is a weak Jahn-Teller effect that splits the singly occupied two-fold degenerate HOMO state originating from Co_2 . This splitting is very small (<1 meV), since the original C_∞ symmetry of the Co dimer where the HOMO resides is only weakly distorted by the hexagonal ligand. Thus, it will hardly have any influence on the magnetic properties of Co_2Bz . In particular, if spin-orbit coupling is taken into account, the HOMO will be split by this interaction rather than by the Jahn-Teller effect, which is almost 2 orders of magnitude weaker than the spin-orbit coupling in the considered case. Only if the magnetization is oriented perpendicular to the dimer axis, the spin-orbit splitting vanishes in lowest order. In this case, the Jahn-Teller effect might marginally reduce the total energy and, thus, the MAE.

We conclude that Co_2Bz and Ni_2Bz probably exhibit a C_{6v} symmetry, like Fe_2Bz . As distinct from the Fe system, Co_2Bz and Ni_2Bz have a stable magnetic ground state. Experimental evidence of these proposed structures seems however lacking at the moment. For the anion Co_2Bz^- , the observed photoelectron spectra²⁴ allowed to exclude a structure where the two Co atoms are placed on both sides of the benzene plane.

2. *4d transition-metal complexes*

We find (Fig. 2) that among the investigated *4d* dimers only Ru_2 prefers an upright adsorption mode. It binds to the benzene as strongly as the cobalt dimer, but its magnetic ground state has a lower spin, $S = 1$, and lies only 0.25 eV below a zero spin state. The ground states of both Rh_2Bz and Pd_2Bz are found to be almost degenerate with respect to spin multiplicity (Rh_2Bz) or geometry (Pd_2Bz).

We are not aware of any published information about the geometry of the neutral complexes Ru_2Bz and Rh_2Bz . For the cation Rh_2Bz^+ , the structure type \parallel_{b} (Fig. 1) was obtained as the lowest-energy structure by DFT calculations using the B3LYP functional.³⁴ This is the same ground-state structure as we find for the neutral Rh_2Bz .

Lüttgens *et al.*²⁹ deduced the vibration energies of both Pd_2Bz and Pd_2Bz^- from photoelectron detachment spectra. They postulated an orientation of the Pd dimer perpendicular to the benzene ring because the observed vibration frequency of Pd_2Bz is close to that of the free Pd_2 . One should note that our calculated ground-state geometry of Pd_2Bz contradicts this analysis. On the other hand, calculations by Cabria *et al.*³⁸ using LSDA and GGA and by Loboda *et al.*³⁹ using the B3LYP functional find a ground-state geometry with the two palladium atoms placed horizontally above the carbon ring, similar to our results.

We performed a series of additional tests in order to clarify this discrepancy between experiment and theory. First, we checked the influence of spin-orbit interaction and found, that related total energy shifts do not exceed 0.1 eV. The parallel adsorption mode hence is still more stable than the perpendicular one. Second, we checked a possible asymmetric adsorption above a single bridge site. Indeed, the related total energy is about 0.5 eV lower than for the adsorption above the hollow site, if every symmetry constraint is released. The dimer axis then deviates from the initial perpendicular orientation and forms an angle of about 40 degrees with the benzene plane, while $S = 0$. Yet, the energy of this structure is still higher than that of the parallel configuration. Third, we calculated vibration frequencies of the Pd-Pd bond using the harmonic approximation for the three adsorption modes defined in Fig. 1. If $S = 1$, the three structures give rise to almost the same vibration energies of 21.9 meV (\perp_{c}), 22.3 meV (\parallel_{b}) and 22.5 meV (\parallel_{t}). For the asymmetric bridge site configuration, a value of 20.6 meV is obtained. All of these energies are close to the vibration energy of the free dimer, 26 meV.⁶¹ This comparison shows that proximity of the vibration spectrum to that of the free dimer is no proof of the perpendicular geometry. For the ground state, $S = 0$, the parallel structures turn out to be much softer, 12.8 meV (\parallel_{b}) and 13.3 meV (\parallel_{t}), than the free dimer and also than the perpendicular geometry, 19.7 meV. On the whole, the calculated vibration spectra do not provide enough evidence in favor of any investigated structure. Finally, we optimized the structures of Pd_2Bz^- anions. The structure \parallel_{b} with $S = 1/2$ is again more stable than the structure \perp_{c} , by 0.45 eV. The structure with asymmetric bonding above a single bridge site is 0.13 eV lower in energy than the structure \perp_{c} , but it is

still 0.32 eV higher than the structure \parallel_b . Summarizing this point, the discrepancy between experimental and theoretical results on Pd_2Bz persists.

B. Electronic structure and bonding mechanism

Free TM dimers have been discussed in detail recently.^{8,11,19,62} Analysis of their electronic structure reveals that a singly occupied HOMO which is two-fold degenerate in the absence of spin-orbit coupling is responsible for the giant magnetic anisotropy predicted in some of these dimers.⁸ For example, the most important feature in Co_2 is a two-fold degenerate singly occupied $3d\text{-}\delta_u^*$ state. It is split by spin-orbit interaction, if the magnetic moment is oriented along the dimer axis but stays degenerate if the moment is oriented perpendicular to the axis.⁸ Concerning the bonding between metal atoms and a benzene molecule, Mokrousov *et al.*⁹ reported a schematic analysis for V-Bz complexes and showed that the HOMO and the lowest unoccupied molecular orbital (LUMO) of benzene interact with the metal s and d orbitals of the same symmetry.

To better understand the bonding mechanism between the TM dimer and the benzene molecule, we compare the levels of Co_2Bz and of Fe_2Bz with those of the related free dimers, Fig. 4. The third panel (from left) shows the textbook electronic structure of benzene and the leftmost panel refers to the free Co_2 , as recently discussed in Ref. 8. The other panels show the electronic structure evaluated for the ground-state geometries and spin multiplicities of Co_2Bz , Fe_2Bz , and Fe_2 as well as for the low-lying $S = 3$ state of Fe_2Bz . It turns out that bonding of Co_2 on benzene does not lead to any deterioration of the magnetic properties of Co_2 : (i) the ground-state spin stays $S = 2$, as in the free dimer; (ii) the Co $3d\text{-}\delta_u^*$ level is still two-fold degenerate in Co_2Bz due to the C_{6v} symmetry; (iii) this level is still the singly occupied HOMO. In this way, the key feature responsible for the giant MAE of the free Co dimer is preserved in the Co_2Bz structure if the benzene molecule binds perpendicularly to Co_2 in C_{6v} symmetry. Yet, there is an important difference between free Co_2 and Co_2Bz . In the free dimer, the two Co atoms contribute equal weights to the minority spin $3d\text{-}\delta_u^*$ state. At variance, the HOMO of Co_2Bz receives 94% of its weight from that Co atom which is farther away from the benzene plane, see Fig. 5.

One can note that the magnetic moment of free Co_2 is also preserved in the parallel arrangements \parallel_b and \parallel_t (Fig. 2). However, the reduction of the symmetry to C_{2v} causes a

split of all δ and π states (not shown here), resulting in non-degenerate HOMO and LUMO in these structures. The minority spin π^* state near to the Fermi level is split by 0.57 eV in the \parallel_b structure and by 0.60 eV in the \parallel_t structure, while the δ^* state in the minority spin channel is split yet more strongly, by 0.68 eV in \parallel_b and by 0.85 eV in \parallel_t .

We find that, unlike in the case of Co_2 , the adsorption of Fe_2 on benzene results in a change of both magnetic moment and electron configuration, as compared with the free Fe dimer. The ground-state level scheme of Fe_2 is very similar to that of Co_2 , see Fig. 4, but two more holes are introduced in the minority spin channel. As a result, $S = 3$ (Fe_2) instead of $S = 2$ (Co_2) and the exchange splitting is enhanced, so that the majority spin $4s\sigma^*$ level is again quasi-degenerate with the HOMO. The latter is now allocated to the singly occupied δ orbital instead of δ^* in Co_2 . If Fe_2 binds to benzene, the electron occupying the majority spin π^* level of Fe_2 moves into the minority spin δ level. The minority spin δ level becomes doubly occupied, while the majority spin π^* level turns singly occupied and acts as the HOMO in the $S = 2$ ground state of Fe_2Bz .

The electronic structure of Fe_2Bz is very similar to that of Co_2Bz in the same spin state ($S = 2$). The covalent splittings of the d -states are somewhat larger in the Fe system than in the Co one, due to the larger extension of the Fe- d orbitals compared with the d -orbitals of Co. This yields a somewhat different orbital order. It will be recalled that in Fe_2Bz a state with $S = 3$ is close in energy to the ground state; in this state the exchange splitting is larger and both holes enter the minority spin channel, like in the free Fe dimer. We included the corresponding level scheme for comparison in Fig. 4. The essential difference between Fe_2 and excited Fe_2Bz in the same spin state is that σ and δ in the minority spin channel interchange their positions. Thus, Fe_2Bz in the state $S = 3$ has a fully occupied δ HOMO and, thus, a small magnetic anisotropy.

The orbital characteristics at the Fermi level determine the main physical properties of the structure, while the stability of the complex depends on how the TM dimer binds to the benzene molecule. Fig. 5 shows the integrated density of states (IDOS) for the ground state of the Co_2Bz structure and the orbital composition of each state.

In an axial symmetry, the five d orbitals are split into three groups: $d\sigma(d_{z^2})$, two-fold degenerate $d\pi(d_{xz}, d_{yz})$, and two-fold degenerate $d\delta(d_{xy}, d_{x^2-y^2})$. The six benzene π orbitals can also be classified with respect to the same axis⁶³ and include one $L\sigma(\pi_1)$ orbital, two degenerate HOMO $L\pi(\pi_2, \pi_3)$, two degenerate LUMO $L\delta(\pi_4^*, \pi_5^*)$, and one $L\phi(\pi_6^*)$ orbital,

where L means ligand. The adsorption between the Co dimer and the benzene molecule is realized primarily by forming three types of chemical bonds, δ , π , and $s\sigma$, between carbon atoms and Co1 (the Co atom nearest to the benzene ring), while the other Co atom, Co2, mainly binds with Co1 and scarcely contributes to the bonding with the benzene. For example, the minority spin δ state at -4.3 eV and the related π^* -dominated ($Bz-L\delta$) δ -state at -1.2 eV in Fig. 5 stem from the combination of the d_{xy} , $d_{x^2-y^2}$ orbitals of Co1 and the LUMO of benzene. The π states positioned near -7.8 eV in the minority spin channel and around -8.0 eV in the majority channel can be attributed to the d_{xz} , d_{yz} orbitals of Co1 and the HOMO of benzene. The hybridization between the $4s$ orbital of Co1 and the $L\sigma(\pi_1)$ orbital of benzene forms the $s\sigma$ orbital, located at around -10.2 eV. Formation of these three kinds of bonds lowers the energy of the Co_2Bz complex compared with the dissociated state and stabilizes the perpendicular adsorption structure.

A simple model for Co_2Bz can be sketched from above analysis of the bond mechanism: the benzene molecule plays the role of a substrate to fix the Co dimer, the Co atom next to the benzene plane acts as “glue” to bind the dimer to the benzene, and the other Co atom mainly contributes to the states near the Fermi level and dominates the magnetic properties of the whole structure.

Level schemes for the ground states of Ni_2Bz , Ru_2Bz and for the related free dimers/benzene are shown in Fig. 6. The electronic structure of Ni_2 is almost unchanged upon adsorption. The spin remains $S = 1$ and π^* of the minority spin channel is still the singly occupied HOMO. The situation is different for Ru_2 , where the total spin is reduced from $S = 2$ to $S = 1$ due to the adsorption. Together with the change of spin, an essential alteration of the orbital order close to the Fermi level takes place. In particular, majority spin σ^* and π^* levels interchange their positions. Thus, Ru_2Bz has a singly occupied δ^* HOMO like Co_2Bz .

C. Spin and orbital moments

Site-resolved spin moments μ_S and orbital moments μ_L for the stable magnetic structures with perpendicular geometry (TM = Fe, Co, Ni, Ru) are listed in Table II. The calculations were carried out within the fully relativistic scheme. The moments are aligned perpendicularly (\perp) or parallelly (\parallel) to the benzene plane, respectively. We checked that the in-plane

anisotropy of the magnetic moments is marginally small and can be safely neglected. The effect of the OP correction is also given for comparison. It is clear that the magnetic moment is mainly distributed between the two transition-metal atoms. The magnetic moment on the C sites is so small that it can be neglected ($|\mu_{S(C)}| < 0.05\mu_B$).

Inspection of the μ_S data reveals that in all four systems the TM2 atom shows a much higher spin moment than the TM1 atom. The relatively high coordination number of TM1, seven, results in a considerable reduction of its spin moment. On the other hand, TM2 is only singly coordinated and thus behaves almost like a free atom. The spin moments of Fe, Co, Ni, and Ru free atoms amount to 4, 3, 2, and 4 μ_B , respectively. The calculated spin moments of the TM2 atoms in $3d$ -TM₂Bz complexes are only 0.5...0.7 μ_B smaller than the corresponding atomic values. In the case of Ru, the TM2 carries only about half of the atomic spin moment. Spin magnetism of $4d$ atoms is in general less stable than that of isoelectronic $3d$ atoms, since the $4d$ intra-atomic exchange (Stoner) integrals are somewhat smaller than the related $3d$ integrals.

Another feature is that the spin moments are nearly the same for both magnetization directions. When the moment orientation switches from \perp to \parallel , the primary effect is a change of the orbital moment of the TM atoms. This fact indicates that the magnetic anisotropy of these systems is closely connected to the anisotropy of the orbital moments.⁶⁴ It is worth noting that in both the Co₂Bz and the Ru₂Bz systems the TM2 atoms show very large orbital moments in the \perp orientation and relatively small values in the \parallel orientation. This is a sign of a large magnetic anisotropy of these systems.

As expected, the calculated moments in Table II show that the OP correction generally increases the orbital moment while scarcely affecting the spin moment. For example, when the OP correction is allowed for, the orbital moments of Co atoms with magnetic moments parallel to the Bz plane are about three times larger than those calculated without the OP correction. This is caused by the very construction of the OP correction scheme, where additional (exchange) energy is gained if the orbital moment is enhanced.^{50,51} In case of perpendicular orientation of the moments with respect to the Bz plane, the orbital moments are less influenced by the OP correction, since spin-orbit coupling alone already provides almost the maximum orbital moment allowed by the given electronic level sequence.

The total orbital moments evaluated for the case when the magnetic moment is parallel to the dimer axis (i.e., perpendicular to the benzene plane) directly reflect the nature of the

HOMO. In the case of Fe_2Bz , Fig. 4, the HOMO is a π^* state in the majority spin channel. Spin-orbit coupling splits this state in such a way that the energy of the $m = -1$ sub-level is reduced (m denotes the magnetic quantum number). This sub-level is consequently occupied, while the $m = +1$ sub-level is empty, and the total orbital moment is close to $-1 \mu_B$. In the case of Co_2Bz , Fig. 4, the HOMO is a δ^* state in the minority spin channel. Spin-orbit coupling splits this state so that the energy of the $m = +2$ sub-level is reduced. Accordingly, $\mu_L \approx 2 \mu_B$. In Ni_2Bz , the HOMO is a δ^* state with both sub-levels occupied. Therefore, the orbital moment nearly vanishes. Finally, in Ru_2Bz the HOMO is a δ state in the minority spin channel with $\mu_L \approx 2 \mu_B$.

D. MAE

After analyzing the spin and the orbital moments in the stable \perp_c TM_2Bz structures, we proceed to another important property of magnetic systems, the MAE. This quantity is in the main focus of the present investigation. In the perpendicular adsorption mode of TM_2 on the benzene molecule, it is natural to consider the MAE as the energy difference between the states with magnetization direction parallel and perpendicular to the benzene plane, Eq. (2).

The first two lines in Table III list our calculated MAE for the stable magnetic TM_2Bz structures with $\text{TM} = \text{Fe}, \text{Co}, \text{Ni}, \text{Ru}$. The data for E_{tot} were obtained by two self-consistent fully relativistic calculations with respective magnetization directions. The values calculated without OP correction should be considered as a lower estimate to the expected MAE, while an upper estimate is obtained by including the OP correction.

Endowed with a large ground-state orbital moment as demonstrated in Sec. IIIC, Co_2Bz and Ru_2Bz show a huge MAE. The lower estimate to the MAE in Co_2Bz is hardly changed in comparison with the free Co dimer.¹¹ This is because the magnetic state and the important features of the electronic structure of Co_2 are not changed by the adsorption. The upper estimate, 334 meV per Co_2Bz molecule, is even higher than the related value for Co_2 (188 meV per dimer). This is due to the almost complete localization of the HOMO on TM_2 in the case of Co_2Bz (Table III, lines three and four). While $\mu_{L(\text{TM}_2)}^\perp \approx 2 \mu_B$ in Co_2Bz (Table II), it is only half as large in the free Co dimer, where by symmetry $\mu_{L(\text{TM}_1)} = \mu_{L(\text{TM}_2)} \approx 1 \mu_B$ in the ground state. The OP correction energy is only half as large in the latter case compared

to the former one, since it is quadratic in the atom-projected μ_L . At variance, the spin-orbit coupling energy is linear in μ_L .

The case of Ru_2Bz is different. We find in the ground state of the free Ru dimer (with $S = 2$) a two-fold degenerate, completely occupied majority-spin $3d - \pi^*$ HOMO and, thus, a small MAE. The spin moment is reduced by the adsorption of Ru_2 on benzene. This causes a change of the electron configuration, resulting in a two-fold degenerate and singly occupied δ^* HOMO with a related huge MAE.

The iron system shows a somewhat smaller MAE, mainly due to the smaller value of $|m|$ of the HOMO. Finally, the Ni system has a fully occupied HOMO that does not contribute to the MAE in lowest order. Nonetheless, the obtained MAE reaches or exceeds the highest known experimental values.^{1,3}

We finally would like to understand the obtained numbers in terms of simple arguments based on perturbation theory,⁸ extended here to include the OP correction. Our consideration is limited to systems with singly occupied, two-fold degenerate HOMO (here, Fe_2Bz , Co_2Bz , and Ru_2Bz). The MAE is approximated by the single-particle energy change of the occupied HOMO level upon changing the direction of magnetization. If the OP correction is included, we call the magnetic anisotropy energy $\text{MAE}_{(\text{SO}+\text{OP})}$, otherwise it is called $\text{MAE}_{(\text{SO})}$. Thus,

$$\text{MAE}_{(\text{SO})} \approx |m| \sum_i (C_{m,d-\text{TM}i}^2 + C_{-m,d-\text{TM}i}^2) \xi_d/2 \quad (3)$$

in first-order perturbation theory. Here, ξ_d is the d -shell spin-orbit parameter and $C_{m,d-\text{TM}i}$ is the projection of one of the HOMO orbitals on the d -orbital of atom $\text{TM}i$ ($i = 1, 2$) with magnetic quantum number m ($|m| = 1$ or 2 for a HOMO of type π or δ , respectively). If OP corrections are taken into account, this first-order estimate changes to

$$\text{MAE}_{(\text{SO}+\text{OP})} \approx |m| \sum_i (C_{m,d-\text{TM}i}^2 + C_{-m,d-\text{TM}i}^2) (\xi_d/2 + B\Delta|\mu_{L(\text{TM}i)}|/\mu_B). \quad (4)$$

Here, B denotes the TM-specific Racah parameters,⁶⁵ evaluated from the related atomic orbitals, and $\Delta|\mu_{L(\text{TM}i)}| = |\mu_{L(\text{TM}i)}^\perp| - |\mu_{L(\text{TM}i)}^\parallel|$, ($i = 1, 2$), according to Tab. II.

Table III shows the major contributions to the composition of the HOMO, ($C_{m,d-\text{TM}i}^2 + C_{-m,d-\text{TM}i}^2$), the related magnetic quantum number $|m|$, the occupation of the HOMO, the spin-orbit parameters, and the Racah parameters. MAE values estimated by first-order perturbation theory are given in brackets following the self-consistently evaluated MAE data. We find that the self-consistent values are smaller than the estimates obtained by

perturbation theory. This has at least two reasons: (i) negative contributions from levels other than the HOMO and higher-order HOMO contributions, cf. the results for Ni_2Bz where the HOMO does not contribute in first order, and (ii) charge relaxation reduces the effect. Nonetheless, the self-consistent MAE amounts to 60 ... 80% of the first-order estimates.

According to the above analysis, Co_2Bz and Ru_2Bz are interesting candidates for strong-MAE applications. It should be noted that in both cases the easy axis of magnetization is directed perpendicularly to the benzene ring. This fact is advantageous for conventional recording techniques.

IV. SUMMARY

We report a systematic DFT study of the ground-state structures, bonding mechanism, spin and orbital moments, and in particular of the MAE of TM_2Bz complexes (TM=Fe, Co, Ni, Ru, Rh, Pd), using the full-potential local-orbital method FPLO. Upright adsorption modes with C_{6v} symmetry of Fe_2 , Co_2 , Ni_2 , and Ru_2 on benzene molecules are confirmed (Fe_2Bz) or predicted (others). Huge MAE, stable geometry, and stable magnetic ground states are predicted for Co_2Bz and for Ru_2Bz . The main origin of the large anisotropy of these two systems is the large orbital moment of the TM atom which is farther away from the benzene plane. Analysis of the electronic states shows that bonding of the Co dimer on the benzene molecule does not lead to any deterioration of the magnetic properties of the dimer. Most important is that the two-fold degenerate singly occupied HOMO state of the free dimer is preserved, which allows the spin-orbit coupling to produce a large magnetic anisotropy. An important conclusion can be drawn from these results: robust and easy-to-prepare carbon-based substrates are well-suited to adsorb transition-metal dimers for the purpose of high-density magnetic recording. We hope that our predicted exceptionally large MAE of Co_2Bz and Ru_2Bz will motivate experimental investigations of transition-metal dimers on carbon-based substrates, like graphite or graphene.

Appendix

A full optimization of all atomic positions was carried out for Co_2Bz complexes by using the ESPRESSO code.⁴⁹ We used the pseudopotentials Co.pbe-nd-rrkjus.UPF, C.pbe-rrkjus.UPF and H.pbe-van_bm.UPF from the <http://www.quantum-espresso.org> distribution. A supercell of the size $20 \text{ \AA} \times 20 \text{ \AA} \times 20 \text{ \AA}$ was used to make sure that there is virtually no interaction between the molecules of neighboring cells. The Brillouin zone sampling was performed only on the Γ point. The cutoffs used for the wave functions and for the charge density were 60 Ry and 300 Ry, respectively. The convergence in total energy was carefully checked. A Marzari-Vanderbilt cold smearing⁶⁶ with 0.007 Ry was used to get the convergence in energy levels. The optimizations were done without any constraints on symmetry or spin moment. Fig. A1 shows the 14 initial structures used to start the geometry optimization.

The optimization results in six types of final structures. Structures (i), (xi), (xii), and (xiii) converge to the perpendicular adsorption mode; structure (x) stays almost unchanged and leads to the parallel adsorption mode on the bridge site of the carbon ring; structures (v) and (ix) converge to the parallel adsorption mode on the top site of the carbon ring; structures (iii), (vi), and (viii) finally go over to a structure type similar to (iii); structures (ii) and (iv) become the structure type (iv); and the final structure of (xiv) is still the adsorption mode on both sides. The optimization for structure (vii) does not converge. Among these structures, the perpendicular adsorption mode shows the lowest total energy, which is 0.74 eV lower than the \parallel_b adsorption mode. The spin of this structure is $S = 2$, confirming the FPLO result. There, the \parallel_b adsorption mode was found 0.98 eV higher than the perpendicular adsorption mode.

Full optimization of all atomic positions shows that there is only a tiny distortion of the benzene plane in the perpendicular adsorption mode. The length of the C-C bonds increases slightly, two of them changing from 1.40 Å to 1.4175 Å and four of them changing to 1.4169 Å. The C-H bond-length changes from 1.09 Å to 1.0889 Å and 1.0887 Å. The electronic structure shows that the two δ^* states (now, HOMO and LUMO) are still nearly degenerate with a gap smaller than 1 meV.

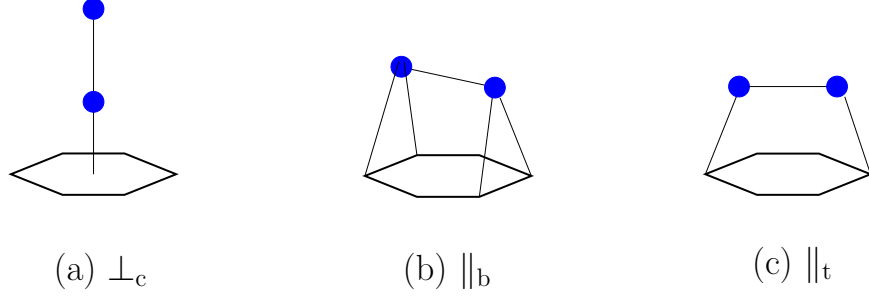


FIG. 1: (Color online) Three possible high-symmetry structures for TM_2Bz complexes. Hexagons and blue bullets indicate benzene rings and transition-metal atoms, respectively. (a) \perp_c – the TM dimer is situated on the C_{6v} symmetry axis perpendicularly to the benzene plane; (b) \parallel_b – the TM dimer is parallel to the benzene plane with TM atoms near the middle of opposite C-C bonds (C_{2v} symmetry); (c) \parallel_t – the TM dimer is parallel to the benzene plane with TM atoms near the top of opposite C atoms (C_{2v} symmetry).

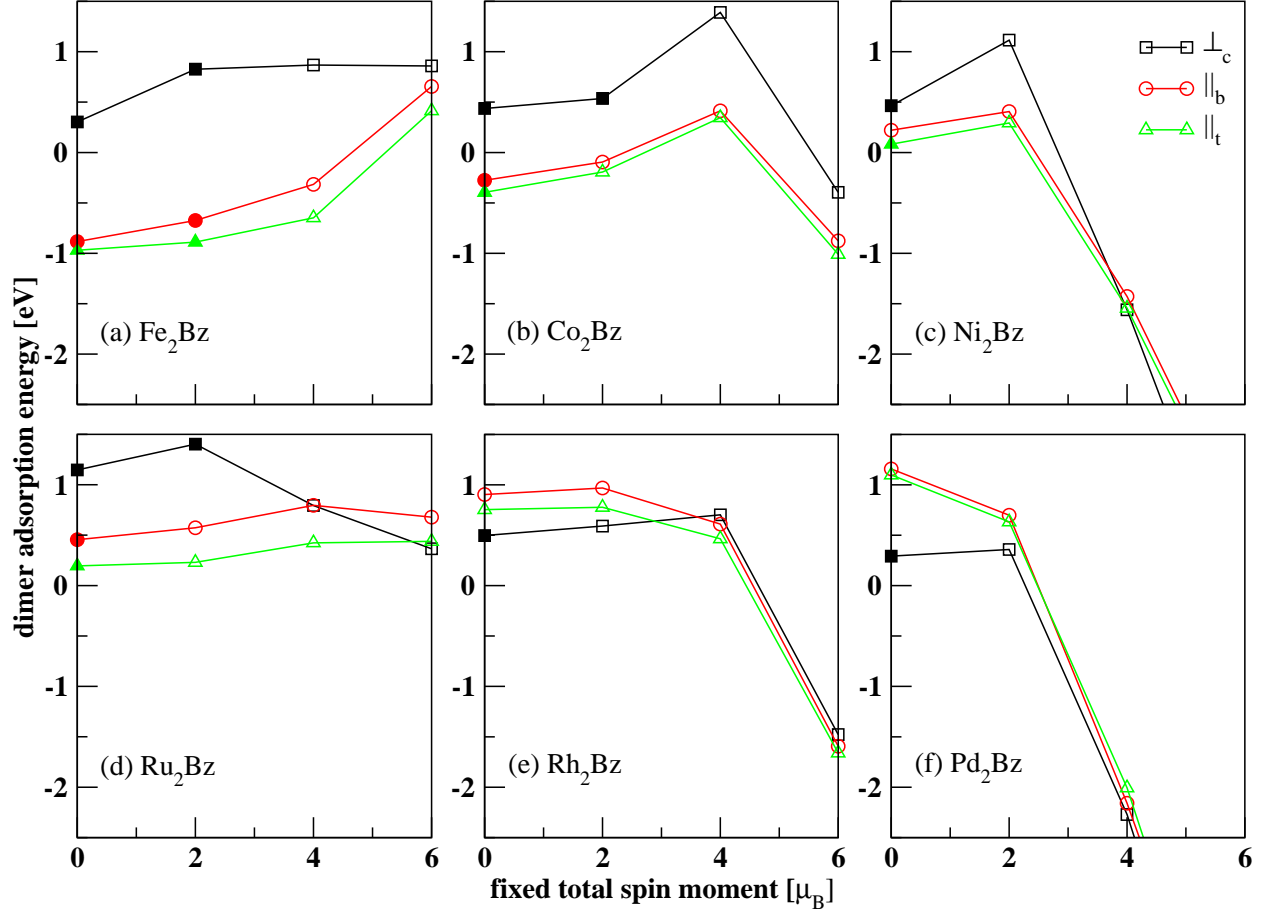


FIG. 2: (Color online) Scalar-relativistic dimer adsorption energies E_{ad} calculated for optimized structures of (a) Fe_2Bz , (b) Co_2Bz , (c) Ni_2Bz , (d) Ru_2Bz , (e) Rh_2Bz , and (f) Pd_2Bz complexes. For all systems, three initial structures illustrated in Fig. 1 were optimized with fixed C and H coordinates for the following values of the fixed total spin moment, $\mu_S=0, 2, 4$, and $6\mu_B$. Both parallel and anti-parallel relative spin orientations were considered. Open (filled) symbols indicate that the moments of the two transition-metal atoms in the spin state with the highest adsorption energy are parallel (anti-parallel).

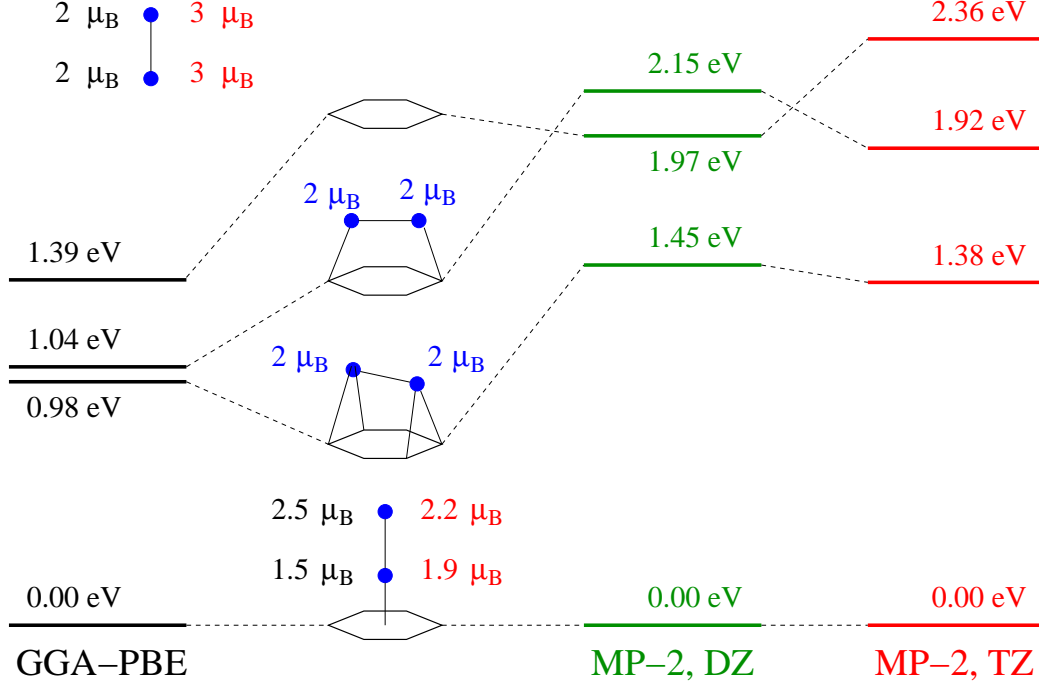


FIG. 3: (Color online) Energies and magnetic moments of different Co_2Bz configurations calculated by DFT (left column) and by MP2 (right columns). DZ and TZ abbreviate double-zeta and triple-zeta basis sets, respectively. The energies refer to the ground-state energy. For the uppermost, dissociated and for the lowermost, ground-state configuration, the spin moments in red (on the right-hand side of the Co dimer) refer to the MP2 calculations and the moments in black (on the left-hand side of the dimer) refer to the GGA calculations. For the other configurations, GGA and MP2 yield the same spin. Hexagons and blue bullets indicate Bz and Co, respectively.

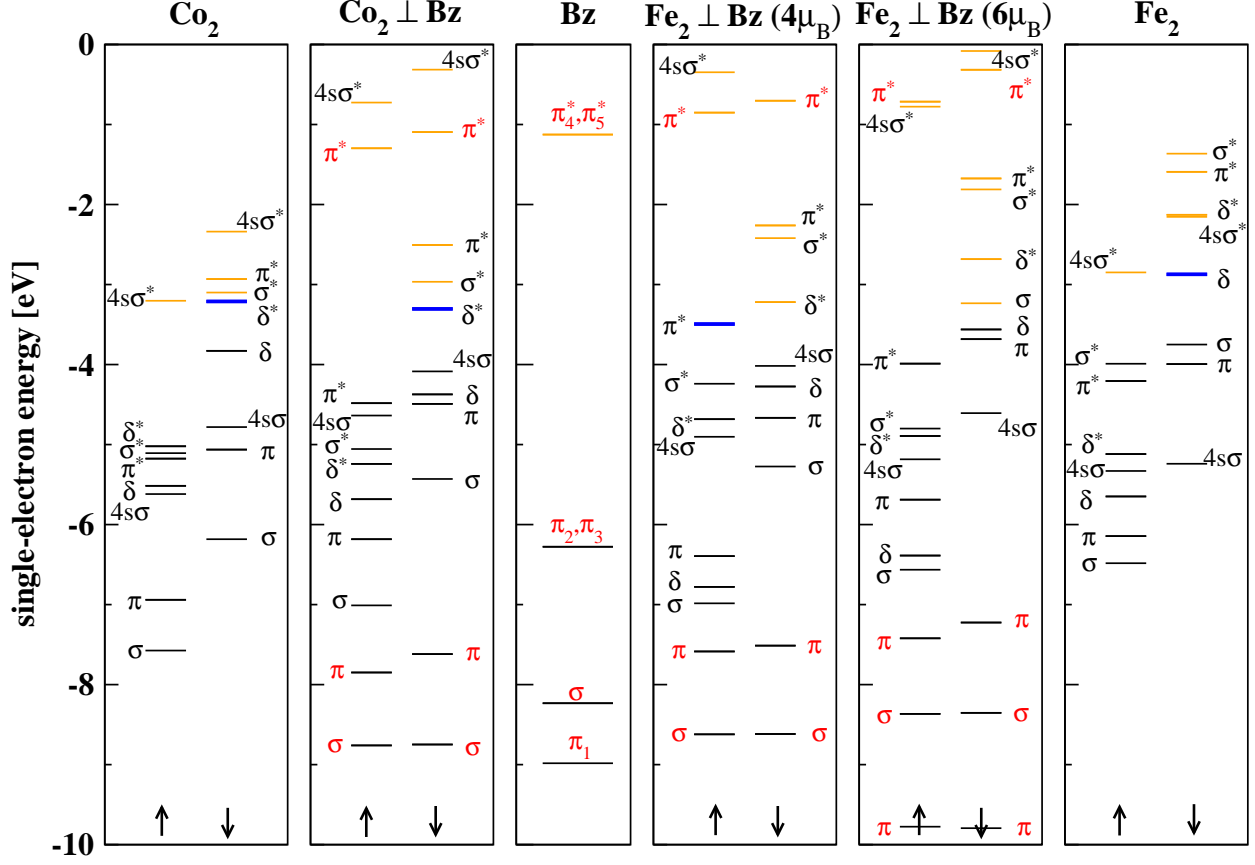


FIG. 4: (Color online) Scalar-relativistic single-particle levels of Co_2 (left panel), Co_2Bz (ground-state structure, second panel), benzene (third panel), Fe_2Bz (ground-state structure, fourth panel and first spin-excited state, fifth panel), and Fe_2 (right panel). All energies refer to a common vacuum level. Black lines denote occupied states, orange (gray) lines denote empty states, and thick blue (gray) lines indicate singly occupied two-fold degenerate states. With the exception of benzene, the levels are spin-split ($S = 2, 2, 2(3)$, and 3 for Co_2 , Co_2Bz , Fe_2Bz , and Fe_2 , respectively). Majority states are indicated by up-arrows, minority states by down-arrows. Dimer-dominated states are labeled in black and benzene-dominated states are labeled in red (gray).

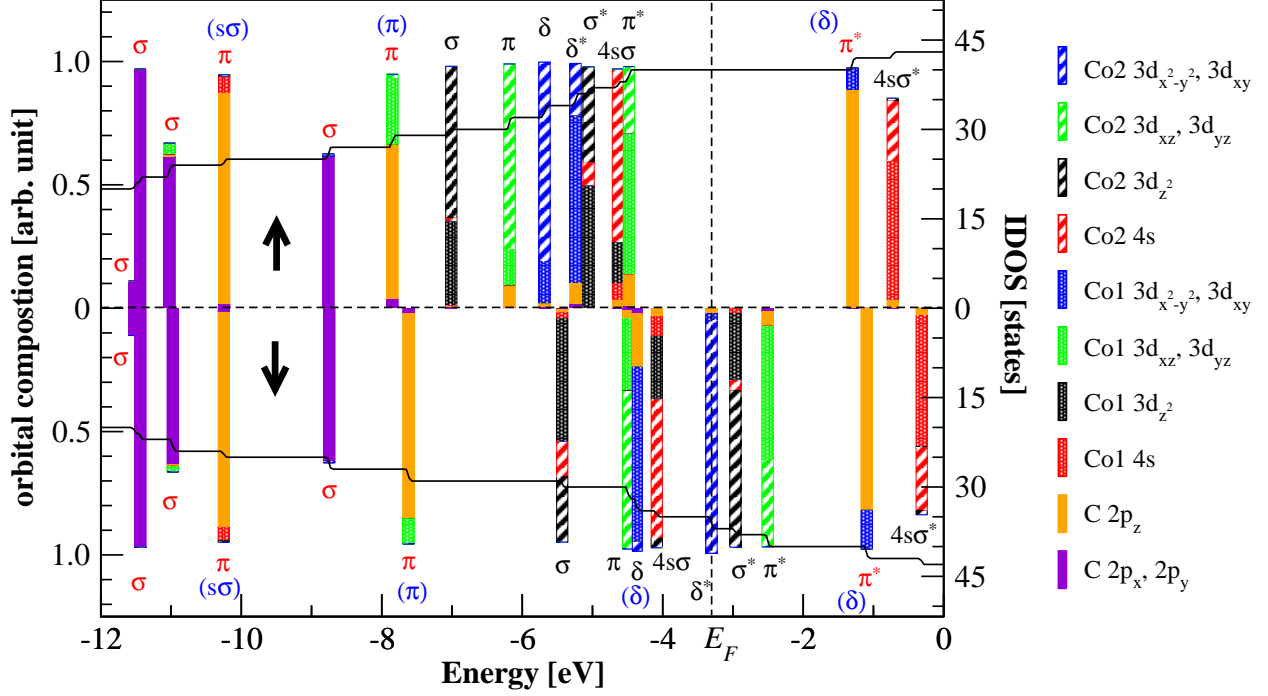


FIG. 5: The orbital composition of each state (left axis) and the integrated density of states (IDOS, right axis) for the ground-state structure and spin of Co_2Bz . The upward (downward) arrow indicates majority (minority) spin states. All energies refer to a common vacuum level. The labels for each state are the same as those in Fig. 4. The three types of chemical bonds between the Co dimer and benzene are labelled blue in parentheses. The Co atom closer to the benzene plane is labelled Co1, the other one is labelled Co2. The position of the Fermi level (E_F) is indicated by a vertical line. Missing contributions to the orbital composition which should add up to unity are due to the omitted C-2s and H-states.

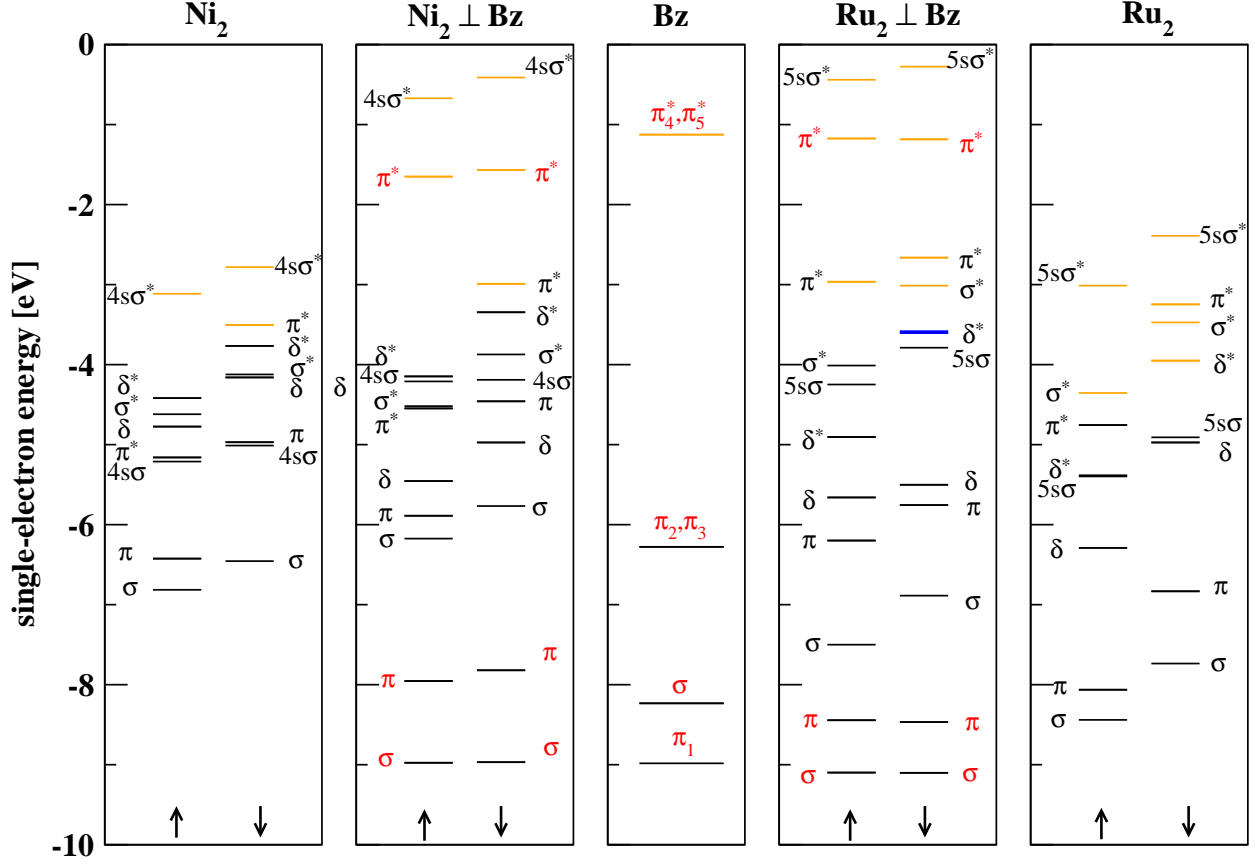


FIG. 6: (Color online) Scalar-relativistic single-particle levels of Ni_2 (left panel), Ni_2Bz (ground-state structure, second panel), benzene (third panel), Ru_2Bz (ground-state structure, fourth panel), and Ru_2 (right panel). All energies refer to a common vacuum level. Black lines denote occupied states, orange (gray) lines denote empty states, and thick blue (gray) lines indicate singly occupied two-fold degenerate states. With the exception of benzene, the levels are spin-split ($S = 1$ in all cases but Ru_2 , where $S = 2$). Majority states are indicated by up-arrows, minority states by down-arrows. Dimer-dominated states are labeled in black and benzene-dominated states are labeled in red (gray).

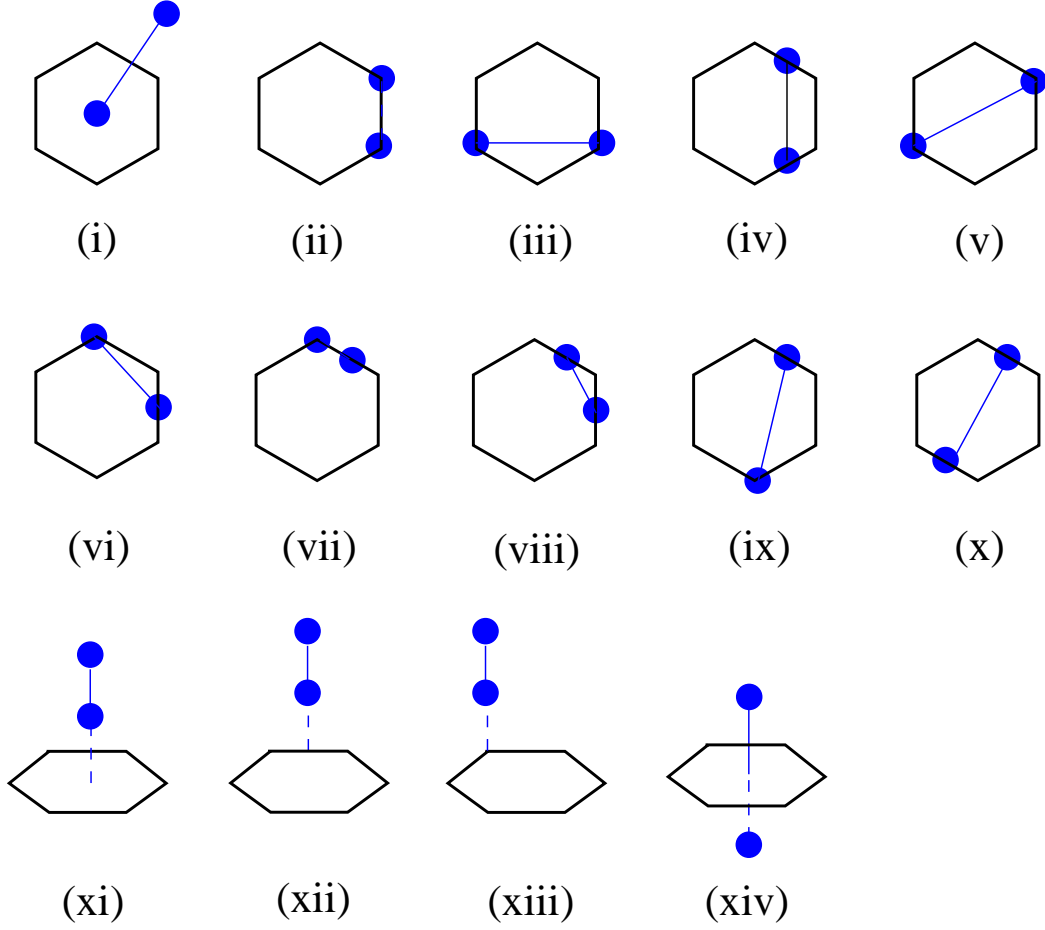


FIG. A1: (Color online) Illustration of 14 initial structures optimized by the ESPRESSO code. From (i) to (x), top-views of possible parallel adsorption modes; from (xi) to (xiii), side-views of possible upright adsorption modes are shown; (xiv) is a case in which one Co atom is attached on each side of the carbon ring.

TABLE I: Dimer adsorption energies, E_{ad} , total and atom-resolved spin magnetic moments, $\mu_{S(\text{total})}$, $\mu_{S(\text{TM1})}$, and $\mu_{S(\text{TM2})}$ (TM1 refers to the atom closer to the benzene in case of perpendicular bonding, TM2 to the other atom), the distance between the two transition-metal atoms $d_{\text{TM-TM}}$, and the distance between benzene plane and TM1, $d_{\text{TM-Bz}}$, for the ground-state structures of TM_2Bz (TM = Fe, Co, Ni, Ru, Rh, Pd) complexes. C-C and C-H bond lengths are fixed (1.40 Å and 1.09 Å, respectively). The structure type of each molecule is labelled according to the notation introduced in Fig. 1. Our present results are labelled “a”, literature data (for dimers on graphene) are labelled “b”, Ref. 40 and “c”, Ref. 38.

system	Fe ₂ Bz		Co ₂ Bz		Ni ₂ Bz		Ru ₂ Bz	Rh ₂ Bz	Pd ₂ Bz	
	a	b	a	b	a	b	a	a	a	c
structure	\perp_c	\perp_c	\perp_c	\perp_c	\perp_c	\perp_c	\perp_c	\parallel_b	\parallel_b	\parallel_b
$E_{ad}(\text{eV})$	0.87	0.72	1.39	0.92	1.12	0.96	1.40	0.97	1.16	1.28
$\mu_{S(\text{total})}(\mu_B)$	4	6	4	4	2	2	2	2	0	0
$\mu_{S(\text{TM1})}(\mu_B)$	0.75	2.76	1.64	1.66	0.71	0.73	-0.10	1.01	0.00	0.00
$\mu_{S(\text{TM2})}(\mu_B)$	3.35	3.48	2.45	2.43	1.29	1.29	2.13	1.01	0.00	0.00
$d_{\text{TM-TM}}(\text{\AA})$	2.04	2.08	2.09	2.03	2.15	2.14	2.22	2.49	2.80	2.75
$d_{\text{TM-Bz}}(\text{\AA})$	1.60	1.86	1.66	1.72	1.71	1.73	1.77	2.08	2.14	2.15

TABLE II: Spin moments μ_S and orbital moments μ_L (in μ_B) for the ground-state structures of TM_2Bz (TM = Fe, Co, Ni, Ru) complexes calculated within the fully relativistic scheme with magnetization perpendicular (\perp) or parallel (\parallel) to the benzene plane. The effect of the OP correction is also illustrated by comparing the values calculated without the OP correction (SO) and with the OP correction (SO+OP).

	Fe_2Bz		Co_2Bz		Ni_2Bz		Ru_2Bz	
	SO	SO+OP	SO	SO+OP	SO	SO+OP	SO	SO+OP
$\mu_{S(\text{TM1})}^\perp$	0.75	0.73	1.64	1.64	0.71	0.71	-0.09	-0.10
$\mu_{S(\text{TM1})}^\parallel$	0.75	0.75	1.64	1.64	0.71	0.67	-0.09	-0.09
$\mu_{L(\text{TM1})}^\perp$	-0.72	-0.89	0.07	-0.10	0.01	0.02	0.04	-0.04
$\mu_{L(\text{TM1})}^\parallel$	0.02	0.05	0.13	0.39	0.04	-0.31	0.03	0.02
$\mu_{S(\text{TM2})}^\perp$	3.34	3.36	2.45	2.46	1.28	1.28	2.13	2.13
$\mu_{S(\text{TM2})}^\parallel$	3.34	3.34	2.45	2.45	1.28	1.33	2.10	2.11
$\mu_{L(\text{TM2})}^\perp$	-0.17	-0.17	1.93	2.12	0.01	0.00	1.91	2.01
$\mu_{L(\text{TM2})}^\parallel$	0.11	0.25	0.17	0.54	0.37	1.69	0.11	0.21
$\mu_{L(\text{total})}^\perp$	-0.89	-1.06	2.00	2.02	0.02	0.02	1.95	1.97
$\mu_{L(\text{total})}^\parallel$	0.13	0.30	0.30	0.93	0.41	1.38	0.14	0.23

TABLE III: The MAE (per molecule), calculated using Eq. (2) for the ground-state structures of TM_2Bz ($\text{TM} = \text{Fe}, \text{Co}, \text{Ni}, \text{Ru}$). Positive values of MAE indicate that the easy axis of the system is perpendicular to the benzene plane, while negative values mean that the direction parallel to the benzene plane is the easy axis. Both a lower estimate of the MAE calculated without OP correction ($\text{MAE}_{(\text{SO})}$) and an upper estimate of the MAE obtained with OP correction ($\text{MAE}_{(\text{SO}+\text{OP})}$) are listed. Data in brackets indicate estimates obtained by first-order perturbation theory, see text. Further, the principal composition $C_{m,d-\text{TM}i}^2 + C_{-m,d-\text{TM}i}^2$, the magnetic quantum number $|m|$, and the occupation of the HOMO are given as well as the spin-orbit coupling parameter ξ_d and the Racah parameter B .

	Fe_2Bz	Co_2Bz	Ni_2Bz	Ru_2Bz
$\text{MAE}_{(\text{SO})}$ (meV)	+15 [+25]	+51 [+74]	-7	+104 [+123]
$\text{MAE}_{(\text{SO}+\text{OP})}$ (meV)	+61 [+107]	+334 [+519]	-96	+279 [+403]
$C_{m,d-\text{TM}1}^2 + C_{-m,d-\text{TM}1}^2$	68%	3%	21%	2%
$C_{m,d-\text{TM}2}^2 + C_{-m,d-\text{TM}2}^2$	15%	94%	77%	94%
$ m $ of the HOMO	1	2	2	2
occupation of the HOMO	1	1	2	1
ξ_d (meV)	61	76	96	128
B (meV)	140	149	154	95

Acknowledgments

Discussions with Helmut Eschrig and with Hway Chuan Kang are gratefully acknowledged.

-
- ¹ P. Gambardella, S. Rusponi, M. Veronese, S. S. Dhesi, C. Grazioli, A. Dallmeyer, I. Cabria, R. Zeller, P. H. Dederichs, K. Kern, C. Carbone, and H. Brune, *Science*, **300**, 1130 (2003).
- ² S. Accorsi, A.-L. Barra, A. Caneschi, G. Chastanet, A. Cornia, A. C. Fabretti, D. Gatteschi, C. Mortalò, E. Olivieri, F. Parenti, P. Rosa, R. Sessoli, L. Sorace, W. Wernsdorfer, and L. Zobbi, *J. Am. Chem. Soc.*, **128**, 4742 (2006).
- ³ C. J. Milios, A. Vinslava, W. Wernsdorfer, S. Moggach, S. Parsons, S. P. Perlepes, G. Christou, and E. K. Brechin, *J. Am. Chem. Soc.*, **129**, 2754 (2007).
- ⁴ M. Mannini, F. Pineider, P. Sainctavit, C. Danieli, E. Otero, C. Sciancalepore, A. M. Talarico, M.-A. Arrio, A. Cornia, D. Gatteschi, and R. Sessoli, *Nature Mater.*, **8**, 194 (2009).
- ⁵ P. Gambardella, S. Stepanow, A. Dmitriev, J. Honolka, F. M. F. de Groot, M. Lingenfelder, S. S. Gupta, D. D. Sarma, P. Bencok, S. Stanescu, S. Clair, S. Pons, N. Lin, A. P. Seitsonen, H. Brune, J. V. Barth, and K. Kern, *Nature Mater.*, **8**, 189 (2009).
- ⁶ H. Stillrich, C. Menk, R. Frömter, and H. P. Oepen, *J. Appl. Phys.*, **105**, 07C308 (2009).
- ⁷ P. Ravindran, A. Kjekshus, H. Fjellvåg, P. James, L. Nordström, B. Johansson, and O. Eriksson, *Phys. Rev. B*, **63**, 144409 (2001).
- ⁸ T. O. Strandberg, C. M. Canali, and A. H. MacDonald, *Nature Mater.*, **6**, 648 (2007).
- ⁹ Y. Mokrousov, N. Atodiresei, G. Bihlmayer, S. Heinze, and S. Blügel, *Nanotechnology*, **18**, 495402 (2007).
- ¹⁰ A. Smogunov, A. D. Corso, A. Delin, R. Weht, and E. Tosatti, *Nature Nanotechnology*, **3**, 22 (2008).
- ¹¹ D. Fritsch, K. Koepernik, M. Richter, and H. Eschrig, *J. Comp. Chem.*, **29**, 2210 (2008).
- ¹² M. E. Gruner, G. Rollmann, P. Entel, and M. Farle, *Phys. Rev. Lett.*, **100**, 087203 (2008).
- ¹³ A. M. Conte, S. Fabris, and S. Baroni, *Phys. Rev. B*, **78**, 014416 (2008).
- ¹⁴ R. Xiao, D. Fritsch, M. D. Kuz'min, K. Koepernik, H. Eschrig, M. Richter, K. Vietze, and G. Seifert, *Phys. Rev. Lett.*, **103**, 187201 (2009).
- ¹⁵ H. Zhang, M. Richter, K. Koepernik, I. Opahle, F. Tasnádi, and H. Eschrig, *New J. Phys.*, **11**, 043007 (2009).
- ¹⁶ S. H. Charap, P.-L. Lu, and Y. He, *IEEE Trans. Magn.*, **33**, 978 (1997).
- ¹⁷ H. Brooks, *Phys. Rev.*, **58**, 909 (1940).

- ¹⁸ L. Fernández-Seivane and J. Ferrer, Phys. Rev. Lett., **99**, 183401 (2007).
- ¹⁹ T. O. Strandberg, C. M. Canali, and A. H. MacDonald, Phys. Rev. B, **77**, 174416 (2008).
- ²⁰ D. J. Trevor, R. L. Whetten, D. M. Cox, and A. Kaldor, J. Am. Chem. Soc., **107**, 518 (1985).
- ²¹ D. W. Ball, Z. H. Kafafi, R. H. Hauge, and J. L. Margrave, J. Am. Chem. Soc., **108**, 6621 (1986).
- ²² W. Zheng, S. N. Eustis, X. Li, J. M. Nilles, O. C. Thomas, K. H. Bowen, and A. K. Kandalam, Chem. Phys. Lett., **462**, 35 (2008).
- ²³ X. Li, S. Eustis, K. H. Bowen, A. K. Kandalam, and P. Jena, J. Chem. Phys., **129**, 074313 (2008).
- ²⁴ M. Gerhards, O. C. Thomas, J. M. Nilles, W.-J. Zheng, and K. H. Bowen, J. Chem. Phys., **116**, 10247 (2002).
- ²⁵ A. K. Kandalam, P. Jena, X. Li, S. N. Eustis, and K. H. Bowen, J. Chem. Phys., **129**, 134308 (2008).
- ²⁶ A. K. Kandalam, B. Kiran, P. Jena, X. Li, A. Grubisic, and K. H. Bowen, J. Chem. Phys., **126**, 084306 (2007).
- ²⁷ W. Zheng, J. M. Nilles, O. C. Thomas, and K. H. Bowen, J. Chem. Phys., **122**, 044306 (2005).
- ²⁸ C. Berg, M. Beyer, T. Schindler, G. Niedner-Schatteburg, and V. E. Bondybey, J. Chem. Phys., **104**, 7940 (1996).
- ²⁹ G. Lüttgens, N. Pontius, C. Friedrich, R. Klingeler, P. S. Bechthold, M. Neeb, and W. Eberhardt, J. Chem. Phys., **114**, 8414 (2001).
- ³⁰ S. F. Parker, J. Phys. Chem. A, **114**, 1657 (2010).
- ³¹ L. Senapati, S. K. Nayak, B. K. Rao, and P. Jena, J. Chem. Phys., **118**, 8671 (2003).
- ³² B. K. Rao and P. Jena, J. Chem. Phys., **117**, 5234 (2002).
- ³³ B. K. Rao and P. Jena, J. Chem. Phys., **116**, 1343 (2002).
- ³⁴ D. Majumdar, S. Roszak, and K. Balasubramanian, J. Chem. Phys., **107**, 408 (1997).
- ³⁵ G. M. Wang, J. J. BelBruno, S. D. Kenny, and R. Smith, Surf. Sci., **541**, 91 (2003).
- ³⁶ R. Varns and P. Strange, J. Phys.: Condens. Matter, **20**, 225005 (2008).
- ³⁷ D. M. Duffy and J. A. Blackman, Phys. Rev. B, **58**, 7443 (1998).
- ³⁸ I. Cabria, M. J. López, and J. A. Alonso, Phys. Rev. B, **81**, 035403 (2010).
- ³⁹ O. Loboda, V. R. Jensen, and K. J. Børve, Fullerenes, Nanotubes, and Carbon Nanostructures, **14**, 365 (2006).

- ⁴⁰ H. Johll, H. C. Kang, and E. S. Tok, Phys. Rev. B, **79**, 245416 (2009).
- ⁴¹ C. Cao, M. Wu, J. Jiang, and H.-P. Cheng, Phys. Rev. B, **81**, 205424 (2010).
- ⁴² J. P. Perdew, K. Burke, and M. Ernzerhof, Phys. Rev. Lett., **77**, 3865 (1996).
- ⁴³ K. Koepernik and H. Eschrig, Phys. Rev. B, **59**, 1743 (1999).
- ⁴⁴ <http://www.fplo.de>.
- ⁴⁵ J. P. Perdew and Y. Wang, Phys. Rev. B, **45**, 13244 (1992).
- ⁴⁶ R. Pandey, B. K. Rao, P. Jena, and J. M. Newsam, Chem. Phys. Lett., **321**, 142 (2000).
- ⁴⁷ R. Pandey, B. K. Rao, P. Jena, and M. A. Blanco, J. Am. Chem. Soc., **123**, 3799 (2001).
- ⁴⁸ M. R. Philpott and Y. Kawazoe, Chem. Phys., **342**, 223 (2007).
- ⁴⁹ P. Giannozzi, S. Baroni, N. Bonini, M. Calandra, R. Car, C. Cavazzoni, D. Ceresoli, G. L. Chiarotti, M. Cococcioni, I. Dabo, A. D. Corso, S. de Gironcoli, S. Fabris, G. Fratesi, R. Gebauer, U. Gerstmann, C. Gougoussis, A. Kokalj, M. Lazzeri, L. Martin-Samos, N. Marzari, F. Mauri, R. Mazzarello, S. Paolini, A. Pasquarello, L. Paulatto, C. Sbraccia, S. Scandolo, G. Schlauser, A. P. Seitsonen, A. Smogunov, P. Umari, and R. M. Wentzcovitch, J. Phys.: Condens. Matter, **21**, 395502 (2009).
- ⁵⁰ H. Eschrig, M. Sargolzaei, K. Koepernik, and M. Richter, Europhys. Lett., **72**, 611 (2005).
- ⁵¹ O. Eriksson, M. S. S. Brooks, and B. Johansson, Phys. Rev. B, **41**, 7311 (1990).
- ⁵² J. Trygg, B. Johansson, O. Eriksson, and J. M. Wills, Phys. Rev. Lett., **75**, 2871 (1995).
- ⁵³ L. Nordström, M. S. S. Brooks, and B. Johansson, J. Phys.: Condens. Matter, **4**, 3261 (1992).
- ⁵⁴ Gaussian 03, Revision C.02, M. J. Frisch et al., Gaussian, Inc., Wallingford CT, 2004.
- ⁵⁵ M. Dolg, U. Wedig, H. Stoll, and H. Preuss, J. Chem. Phys., **86**, 866 (1987).
- ⁵⁶ T. H. Dunning, Jr., J. Chem. Phys., **90**, 1007 (1989).
- ⁵⁷ S. F. Boys and F. Bernardi, Mol. Phys., **19**, 553 (1970).
- ⁵⁸ S. Simon, M. Duran, and J. J. Dannenberg, J. Chem. Phys., **105**, 11024 (1996).
- ⁵⁹ T. Kurikawa, H. Takeda, M. Hirano, K. Judai, T. Arita, S. Nagao, A. Nakajima, and K. Kaya, Organometallics, **18**, 1430 (1999).
- ⁶⁰ J. R. Lombardi and B. Davis, Chem. Rev., **102**, 2431 (2002).
- ⁶¹ J. Ho, M. L. Polak, K. M. Ervin, and W. C. Lineberger, J. Chem. Phys., **99**, 8542 (1993).
- ⁶² P. Błński and J. Hafner, Phys. Rev. B, **79**, 224418 (2009).
- ⁶³ T. Yasuike and S. Yabushita, J. Phys. Chem. A, **103**, 4533 (1999).
- ⁶⁴ P. Bruno, Phys. Rev. B, **39**, 865 (1989).

⁶⁵ B. R. Judd, *Operator Techniques in Atomic Spectroscopy* (McGraw-Hill, New York, 1963).

⁶⁶ N. Marzari, D. Vanderbilt, A. De Vita, and M. C. Payne, Phys. Rev. Lett., **82**, 3296 (1999).